CORRECTION FOR AMPLIFIER-INDUCED PHASE LAG IN CAPACITANCE GAGE MEASUREMENTS

Vasishta Ganguly and Tony L. Schmitz
Department of Mechanical Engineering and Engineering Science
University of North Carolina at Charlotte
Charlotte, NC, USA

INTRODUCTION

The dynamic response of mechanical structures may be represented by their complex frequency response function (FRF). The FRF is characterized by the frequency dependent magnitude and phase, or real and imaginary parts, which relate the structures response to a force input. The FRF of a structure may be measured using modal testing [1]. In one type of modal testing, referred to as impact testing, an impulse force is applied to a structure and a linear transducer is used to measure the response. The displacement, velocity, or acceleration may be used to identify the FRF.

Capacitance gages and laser Doppler vibrometers (LDV) are non-contact sensors which offer high bandwidth and resolution. These sensors may be used for displacement/velocity feedback, spindle error motion characterization, and frequency response measurements in structural dynamics testing. They employ amplifying electronics to convert the change in displacement/velocity to a proportional voltage which may then be sampled by a data acquisition (DAQ) system. Depending on its design, the amplifier can induce a time delay in the measurement signal, i.e., there is a small time delay between the input displacement/velocity of the target and the output voltage from the amplifier. These time delays lead to frequency dependent phase errors in the FRF. Furthermore, the digital DAQ system may introduce some synchronization errors between the force and response signals.

In this research, an experimental technique to identify the frequency dependent phase error is described. The technique may also be extended to identify synchronization errors due to the DAQ system. A frequency domain approach is proposed to correct the FRF for the phase errors. The method is verified using a standard artifact mounted in a test stand.

EXPERIMENTAL SETUP

Two different methods were employed to evaluate the time delays: a) frequency-sweep test; and b) broadband excitation.

Frequency Sweep Test

In the frequency sweep test, the measurement bandwidth was divided into a number of discrete steps and the phase error was measured independently at each frequency. The amplifier-induced phase error was evaluated by measuring the phase shift between two transducers attached to an oscillating target: a “known” accelerometer and a capacitance gage system. The target was vibrated using a modal shaker (TIRAvib 51075) capable of generating oscillations up to 5000 Hz. A function generator (Hewlett Packard 33120A) was used to drive the shaker at the desired fixed frequency. The target motion was measured using both a low-mass integrated circuit PZT (ICP) accelerometer (PCB 352C23) and a capacitance gage sensor (Lion Precision C23 B). The capacitance gage signal was amplified using a Lion Precision CPL 290 Elite series amplifier. The amplifier bandwidth was set to 15 kHz. Data was acquired at 100 kHz using a NI DAQ card.

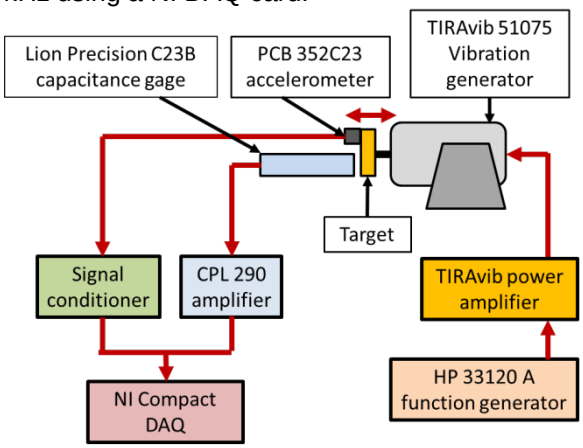

FIGURE 1. Schematic representation of the experimental setup.

Figure 1 shows a schematic representation of the measurement setup. The phase shift, θ, between two time domain sinusoidal signals, x and y, with frequency, ω, may be calculated using:

$$\theta(\omega) = \cos^{-1}\left(\frac{x.y}{|x||y|}\right). \quad (1)$$

Measurements were conducted over a frequency range of 100 Hz to 5000 Hz in 100 Hz increments. The measured data was digitally filtered using a 3rd order band pass filter with a bandwidth of 100 Hz centered at the oscillation frequency. Figure 2 shows the measured phase lag as a function of the oscillation frequency. Within the measured bandwidth, the phase lag changed linearly with respect to the oscillating frequency at a rate of -12.9 deg/kHz, which is consistent with the manufacturer-reported value [2]. Scatter from the best fit line in the 1000 Hz to 2000 Hz range was attributed to compliance in the wax interface between the accelerometer and target, but additional testing is warranted.

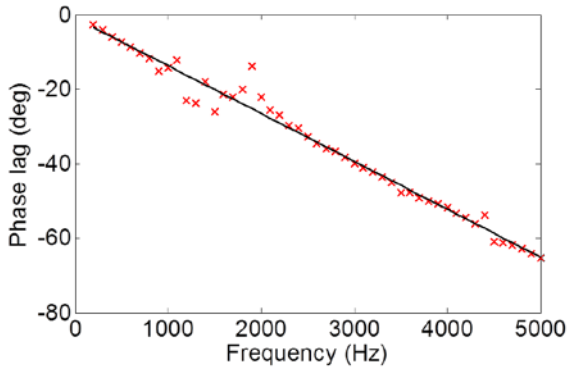

FIGURE 2. Measured phase lag as a function of oscillating frequency.

Broadband Excitation

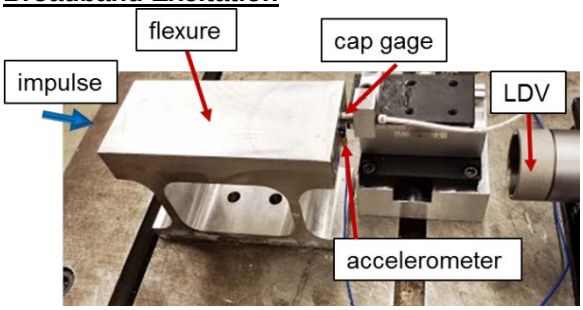

FIGURE 3. Broadband excitation setup.

Figure 3 shows the measurement setup. An impulse force, applied using a modally tuned hammer (PCB 086C04), was used to excite a flexure over a wide frequency range. The response of the flexure was simultaneously measured using an ICP accelerometer (PCB 352C23) which measured acceleration, a LDV (Polytec OFV – 534) which measured velocity, and a capacitance gage (Lion Precision C5 D) which measured displacement. The accelerometer signal was used as the reference signal for the phase error evaluation. The FRF can be expressed in terms of the displacement, velocity, and acceleration signals as:

$$FRF = \frac{X(\omega)}{F(\omega)} = \frac{1}{i\omega}\frac{V(\omega)}{F(\omega)} = -\frac{1}{\omega^2}\frac{A(\omega)}{F(\omega)}, \quad (2)$$

where $X(\omega)$, $V(\omega)$, $A(\omega)$, and $F(\omega)$ are the fast Fourier transforms (FFTs) of the displacement, velocity, acceleration and force signals respectively and ω is the frequency in rad/s. The phase errors introduced by the capacitance gage and LDV amplifying electronics are identified in the frequency domain by comparison with the accelerometer phase.

The excitation bandwidth is inversely related to the impulse period, while the excitation magnitude is directly related to the magnitude of the impulse force. Figure 4 shows a plot of the force FFT magnitude to provide an estimate of the excited bandwidth.

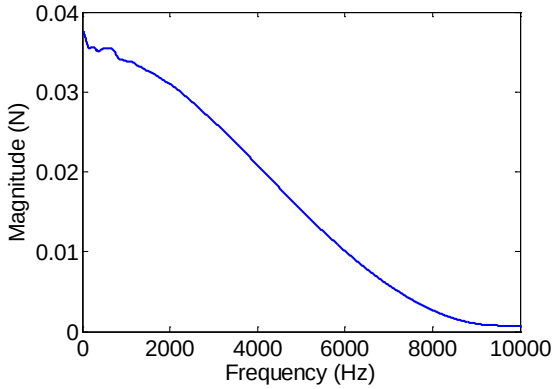

FIGURE 4. Magnitude of impulse force represented in the frequency domain.

Figure 5 shows the first two modes of vibration of the flexure. The three sensors simultaneously measure the dynamics response at different locations on the side of the flexure as shown in Figure 3. The response measured by the three sensors around the first natural frequency (1708 Hz) has the same magnitude and phase. However, for the second (twisting mode) natural

frequency (3400 Hz), the response measured by the three sensors is not necessarily identical. Therefore, the frequency range from 3200 Hz to 3600 Hz was ignored when comparing the phase of the three sensors.

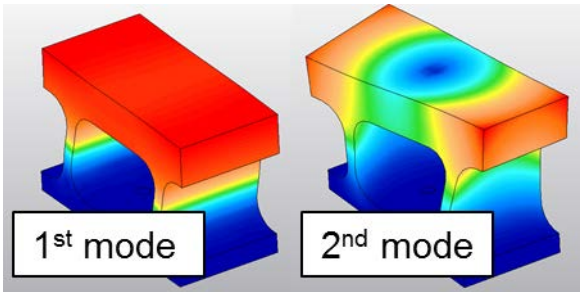

FIGURE 5. First two vibration modes for the flexure.

The coherence of a FRF provides an estimate of the reliability of the measurement [1]. Ideally, the coherence is unity. Figure 6 shows a plot of the FRF coherence for the three sensors. It is less than one at low frequencies for the accelerometer and LDV due to the frequency domain integration. It was also observed that the coherence drops near the second natural frequency. The phase error was only calculated for frequency values where the coherence was greater than 0.95.

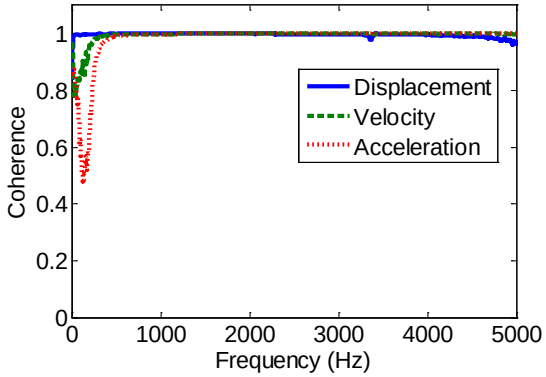

FIGURE 6. FRF coherence: displacement, velocity, and acceleration.

Figure 7 shows the mean phase for the three sensors from 12 repetitions. It is observed that the phase of both the capacitance gage and the LDV lags the accelerometer phase. The frequency dependent phase error is calculated using:

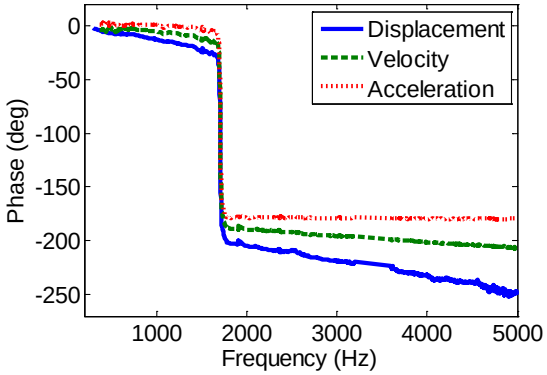

FIGURE 7. FRF phase: displacement (CG), velocity (LDV), and acceleration.

$$\phi_{err_{CG}} = \angle\left(\frac{X(\omega)}{F(\omega)}\right) - \angle\left(-\frac{1}{\omega^2}\frac{A(\omega)}{F(\omega)}\right), \text{ and,}$$

$$\phi_{err_{LDV}} = \angle\left(\frac{1}{i\omega}\frac{V(\omega)}{F(\omega)}\right) - \angle\left(-\frac{1}{\omega^2}\frac{A(\omega)}{F(\omega)}\right), \qquad (3)$$

where∠ represents the FRF phase. Figure 8 shows the frequency dependent phase error for the capacitance gage and LDV measurements. Within the measured bandwidth, the phase error was found to change linearly with frequency. The slope of the linear fit was used to characterize the phase error as shown in Table 1. Note that for the capacitance gage amplifier, the slope derived using the broadband excitation method is 4% higher than that derived using the frequency sweep test. Also note that the capacitance gage phase error is sensitive to the operating bandwidth of the capacitance gage amplifier (CPL 290). In this study, the amplifier was set to a bandwidth of 15 kHz.

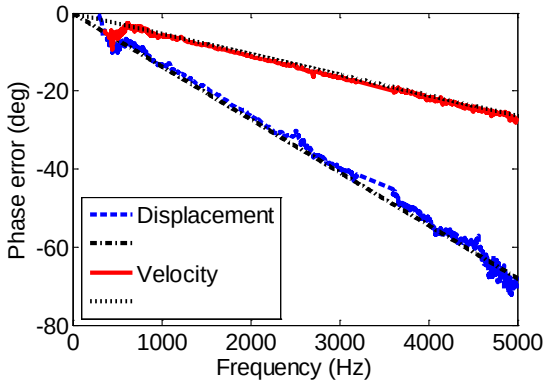

FIGURE 8. Phase error for the capacitance gage and LDV with reference to the accelerometer.

TABLE 1. Slope of frequency dependent phase error.

Instrument	Frequency dependent phase error (deg/kHz)	
	Mean	Standard deviation
Frequency sweep		
Capacitance gage	-12.9	-
Broadband excitation		
Capacitance gage	-13.54	0.165
LDV	-5.47	0.1283

SYNCHRONIZATION ERRORS IN DATA ACQUISITION SYSTEMS

In this study, a National Instrument compact data acquisition system (NI cDAQ 9174) was used to collect the data. Two different cards (NI 9215 and NI 9324) were mounted in the same cDAQ chassis. The NI9215 is capable of measuring a voltage signal within a range of ±10 V at a sampling rate of up to 100 kHz. The NI9324 can measure a voltage signal within the range of ±5 V at a sampling rate of up to 51.2 kHz. The NI9324 also provides the necessary supply current for integrated circuit PZT (ICP) sensors, such as accelerometers and modal hammers. Individually, each card has four channels which are sampled simultaneously. However, the different cards mounted within the same cDAQ chassis are not necessarily synchronized. Synchronization errors between the different channels of the data acquisition system must be taken into account when measuring dynamic response data.

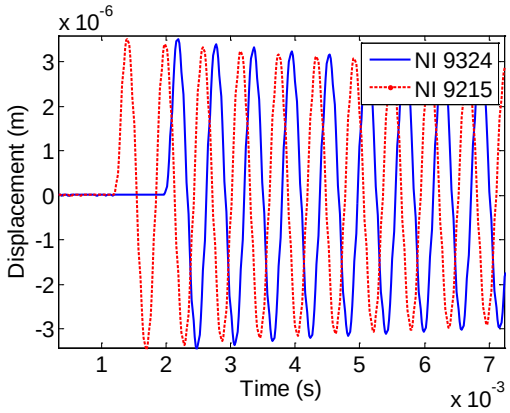

FIGURE 9. Synchronization error in data acquired by two DAQ cards (NI 9215 and NI 9324).

To measure the DAQ system induced synchronization error, the same displacement (response) signal from the capacitance gage was split and was simultaneously collected by both the DAQ cards (NI9215 and NI9324) mounted in the cDAQ chassis. Figure 9 shows a time domain plot of the identical response signal acquired by the two different DAQ cards. The measurement data acquired by the NI9215 card leads that acquired by the NI9324 card. In the frequency domain, the phase delay introduced by the data acquisition system may be estimated as:

$$\phi(\omega) = \angle\left[\frac{X_{NI\,9324}(\omega)}{X_{NI\,9215}(\omega)}\right], \qquad (4)$$

where $X_{NI9324}(\omega)$ and $X_{NI9215}(\omega)$ represent the FFTs of the response signal acquired by the NI9324 and NI9215 DAQ cards, respectively. Figure 10 shows the phase error as a function of frequency. Note that the error is reset to zero each time it is crosses 360 degrees. The NI9324 card lags the NI9215 card.

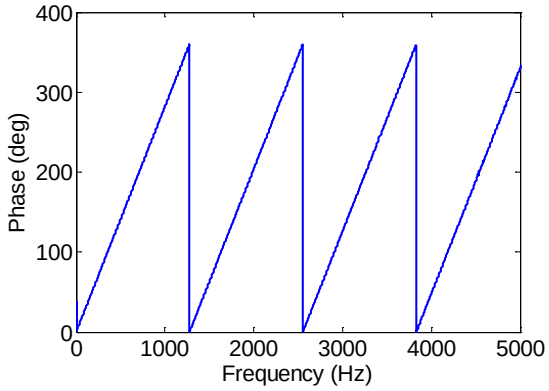

FIGURE 10. DAQ induced phase error.

When measuring the FRF of a mechanical structure, it is necessary to account for the synchronization errors introduced due to the DAQ system as well as the sensor electronics. In this example, the dynamic response of the flexure assembly was measured. The input impulse force signal from the modal hammer was collected by the ICP compatible NI9324 card and the response signal was collected by the NI9215 card. Note that in this case, the impulse data (NI9324) lags the response data (NI9215) which is physically impossible. Also, the capacitance gage amplifier introduced a time delay in the response signal. The phase lag introduced by the capacitance gage amplifier

was smaller than the phase lead introduced by the DAQ system. Both these factors were accounted for when correcting the FRF. Figure 11 shows the net effect of the phase errors introduced by the DAQ system and the capacitance gage amplifier. Figure 12 shows measured and corrected phases for the FRF measurement. Note that the FRF amplitude is constant.

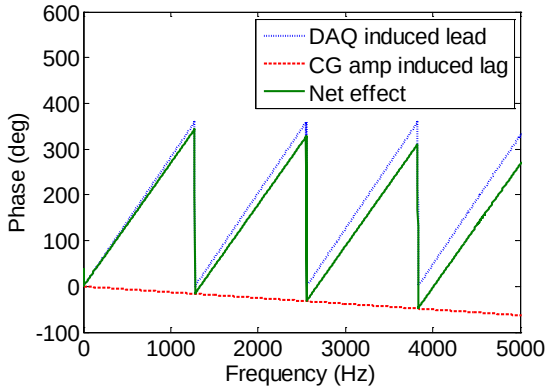

FIGURE 11. Net effect of DAQ and amplifier induced phase errors.

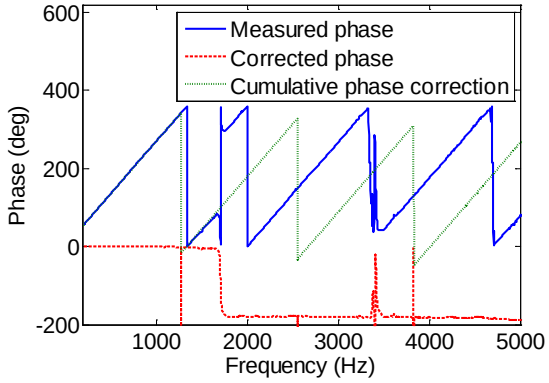

FIGURE 12. Measured and corrected phase of flexure FRF.

CORRECTION FOR FRF PHASE LAG

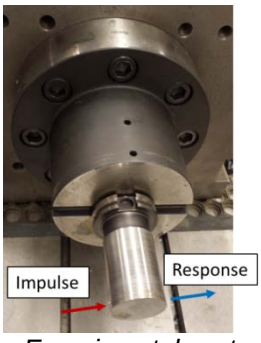

FIGURE 13. Experimental setup to validate phase correction algorithm.

FRF tests were performed at the tip of a standard artifact mounted in a spindle test stand; see Figure 13. A modally tuned hammer (PCB 086C04) was used to apply an impulse force to the artifact and the response was measured using a capacitance gage (Lion Precision C5D), the LDV (Polytec OFV – 534), and an accelerometer (PCB 352C23) sequentially. The data was acquired at 51.2 kHz. All the signals were acquired using the same DAQ card (NI9324) to avoid any DAQ induced synchronization errors. For any FRF, the measured frequency-dependent phase difference between the input force and the output response is:

$$\phi(\omega) = \tan^{-1}\left[\frac{\mathrm{Im}\{FRF(\omega)\}}{\mathrm{Re}\{FRF(\omega)\}}\right], \qquad (5)$$

where Re indicates the real part and Im indicates the imaginary part of the complex FRF. The (linear) phase difference is corrected to account for the amplifier induced phase lag using:

$$\phi(\omega)_{corr} = \phi(\omega)_{meas} - \Delta\theta * \omega, \qquad (6)$$

where $\Delta\theta$ is the rate of change of phase lag with frequency (the slope of the line in Fig. 2).The corrected Re and Im parts of the FRF may then be computed using:

$$\mathrm{Re}(FRF)_{cor} = |FRF(\omega)| * \cos(\phi(\omega)_{corr}), \qquad (7)$$

$$\mathrm{Im}(FRF)_{cor} = |FRF(\omega)| * \sin(\phi(\omega)_{corr}),$$

where $|FRF(\omega)|$ is the FRF magnitude, which is not affected by the phase lag. Figure 14 shows a Nyquist plot of the measured and corrected FRFs obtained using the accelerometer, the capacitance gage and the LDV. In the Nyquist plot, a phase error is manifested as a “rotation” of the Nyquist curve. The corrected curves align with the FRF obtained using the accelerometer. Errors in the magnitude of the real and imaginary parts of the corrected Nyquist plot may be attributed to errors in calibrating the sensor sensitivities.

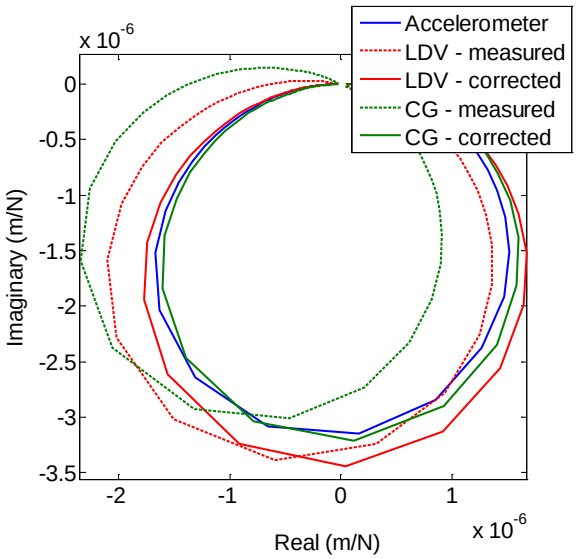

FIGURE 14. Comparison of FRFs obtained using the capacitance gage, LDV, and accelerometer.

CONCLUSIONS

In this study, the frequency dependent phase error induced by the amplifying electronics was identified for a capacitance gage sensor and a laser Doppler vibrometer. Synchronization errors introduced by the data acquisition system was also identified. A frequency domain technique to correct the phase error was described and applied to FRF measurements of a standard artifact in a test stand. The measurements showed that the corrected FRFs agreed with the FRF measured using the accelerometer.

REFERENCES

[1] Ewins D.J, Modal Testing: Theory, Practice and Application, 2nd ed., Research Studies Press LTD, Hertfordshire, 2000.

[2] Lion Precision, TechNote LT03-0031 EliteSeries Amplitude/Phase Frequency Response, 2011.